NASA Contractor Report 191482
ICASE Report No. 93-32

# ICASE

20 Years of Excellence

# PINCHING SOLUTIONS OF SLENDER CYLINDRICAL JETS

**Demetrios T. Papageorgiou**
**Oscar Orellana**



NASA Contract Nos. NAS1-19480, NAS1-18605
June 1993

Institute for Computer Applications in Science and Engineering
NASA Langley Research Center
Hampton, Virginia 23681-0001

Operated by the Universities Space Research Association


National Aeronautics and
Space Administration

**Langley Research Center**
Hampton, Virginia 23681-0001

## ICASE Fluid Mechanics

Due to increasing research being conducted at ICASE in the field of fluid mechanics, future ICASE reports in this area of research will be printed with a green cover. Applied and numerical mathematics reports will have the familiar blue cover, while computer science reports will have yellow covers. In all other aspects the reports will remain the same; in particular, they will continue to be submitted to the appropriate journals or conferences for formal publication.

# PINCHING SOLUTIONS OF SLENDER CYLINDRICAL JETS

*Demetrios T. Papageorgiou*[1]
Department of Mathematics
Center for Applied Mathematics and Statistics
New Jersey Institute of Technology
Newark, New Jersey 07102

and

*Oscar Orellana*[2]
Department of Mathematics
Universidad Federico Santa Maria
Valparaiso, Chile

## ABSTRACT

Simplified equations for slender jets are derived for a circular jet of one fluid flowing into an ambient second fluid, the flow being confined in a circular tank. Inviscid flows are studied which include both surface tension effects and Kelvin-Helmholtz instability. For slender jets a coupled nonlinear system of equations is found for the jet shape and the axial velocity jump across it. The equations can break down after a finite time and similarity solutions are constructed, and studied analytically and numerically. The break-ups found pertain to the jet pinching after a finite time, without violation of the slender jet ansatz. The system is conservative and admissible singular solutions are those which conserve the total energy, mass and momentum. Such solutions are constructed analytically and numerically, and in the case of vortex sheets with no surface tension certain solutions are given in closed form.

[1]This research was supported by the National Aeronautics and Space Administration under NASA Contract Nos. NAS1-19480 and NAS1-18605 while the author was in residence at the Institute for Computer Applications in Science and Engineering (ICASE), NASA Langley Research Center, Hampton, VA 23681.

[2]This research was supported in part by Fondo Nacional de Desarrollo Cientifico y Tecnologico (FONDECYT) under grant No. 246/91 and Universidad Tecnica Federico Santa Maria, Valparaiso, Chile.

# 1 Introduction

Rayleigh [1] first studied the break-up of liquid jets in air. The underlying instability mechanism is a consequence of surface tension, and Rayleigh predicted that all waves longer than the jet diameter are linearly unstable and used the result to conjecture the break-down of the jet into drops. The physics of the instability can be understood in purely energetic terms since for a given stationary volume of fluid the surface energy is a minimum when the shape is spherical. A liquid thread, therefore, will tend to break up into drops. An equivalent and more quantitative feature of the instability is found also by consideration of the Young-Laplace equation which relates the pressure jump across the jet interface to its curvature. In cylindrical geometries we have two principal radii of curvature, one in a plane containing the axis of the jet and one in a plane perpendicular to the axis. If we suppose that a perturbation causes the jet radius to decrease slightly, then the radius of curvature in the cross-sectional plane decreases and the pressure in the vicinity of the perturbation increases. This means that fluid will tend to leave this high pressure region to flow to lower pressure positions, which by mass conservation decreases the jet radius further thus enhancing the interfacial instability. This is a physical description of the mechanism of pinching or break-up. Clearly the phenomenon is nonlinear and even though linear theory does well in predicting dominant wavelengths in natural transition, nonlinear analyses are required to follow the jet to break-up for a range of dominant length scales whether self-sustained or externally imposed through initial conditions for example.

The physical picture sketched above is fundamental and appears in both inviscid as well as viscous flows. In this work we concentrate on inviscid irrotational flows of liquid jets. A review article has been written by Bogy [2]. Of relevance is also the work of Chandrasekhar [3] and some experimental pictures of jet break-up can be found in Donnelly and Glaberson [4] (see also Drazin and Reid [5]). A theoretical study of the break-up of an inviscid incompressible liquid jet in air with surface tension has been carried out by Ting and Keller [6] (referred to as [TK]). The authors make a slender jet approximation where the radial length scale is taken to be much smaller than the axial length scale so that their ratio forms a small parameter which is used in an asymptotic theory to develop a system of one-dimensional coupled PDE's. Similar ideas have also been used by Papageorgiou and Smith [7] in the study of the nonlinear evolution of plane wakes. The evolution equations of [TK] are simpler than the original system making them amenable to an analysis that produces families of pinching solutions which are physically relevant. Self-similar solutions in turn transform the PDE's into ODE's and numerical or exact solutions are given.

The problem studied here is an extension of [TK]. In [TK] the cylindrical jet flows in air.

Within the framework of the Euler equations the undisturbed velocity field is a constant axial velocity which can be removed from the problem by a suitable Galilean transformation. The mechanism of three-dimensional Kelvin-Helmoltz instability is absent and surface tension dominates. Our interest lies in the competing effects of capillary instability and Kelvin-Helmholtz instability which is present if the surrounding (without loss of generality ambient) fluid is of non-zero density. Recently there has been a lot of interest in the formation of singularities in cylindrical vortex sheets. Linear stability studies include the work of Rotunno [8] and more recently singularity formation studies have been undertaken by Caflisch [9], Caflisch and Li [10], Caflisch, Li and Shelley [11], Grauer and Sideris [12], who do not include surface tension but include a background swirl in the azimuthal direction. The flows in [9]-[11] do not possess a jump in axial velocity at the sheet surface and are shown in [8] and [11] to be linearly stable to short waves in the case of axisymmetric disturbances. The problem studied here omits swirl and includes axial velocity jumps which contribute a Kelvin-Helmholtz instability for axisymmetric disturbances. Axisymmetric flows are more likely to form pinching singularities since the axisymmetry prevents the core from flattening out. Even though we do not include swirl in our study we do enforce axisymmetry, and our slender jet equations predict self-similar pinching of the jet even in the absence of surface tension. Such solutions may be suitable candidates for initializing full-scale computations.

The rest of the paper is organized as follows. Section 2 derives the slender jet equations. For completeness we derive a system for fluids of different densities with the axis of the jet being vertical. There, we also describe some useful transformations that reduce the number of unknowns in the evolution equations from three to two which are also more relevant physically. Section 3 discusses properties of the equations including conserved quantities, equation type and linear stability characteristics. According to linear theory, stability windows exist for certain values of density ratios and certain undisturbed jet to pipe radius ratios. Equal density flows are always linearly unstable. In Section 4 we consider the possibility of finite-time singularities and derive the self-similar governing equations. In Section 5 we solve these equations for vortex sheets in the absence of surface tension and give families of exact solutions, and in Section 6 we address the problem including surface tension. Section 7 is devoted to discussion.

# 2 Derivation of the evolution equations

Consider the irrotational flow of an axisymmetric jet of density $\rho_1$ and potential $\phi_1(t,r,z)$ whose bounding surface is $S(t,z)$. The flow outside is also irrotational and is taken to have potential $\phi_2(t,r,z)$ and density $\rho_2$. The flow takes place in a vertical arrangement

with gravity acting and there is an outer bounding solid surface at $r = R_2$ (a cylindrical polar coordinate system $(r, \theta, z)$ is used throughout with the corresponding velocity field $\mathbf{u} = (u, v, w)$). If in addition surface tension acts and the tension coefficient is constant, $\sigma$ say, the following piecewise constant solution of the Euler equations is available:

$$\mathbf{u}_1 = (0, 0, W_0) \quad 0 < r < R_1,$$

$$\mathbf{u}_2 = (0, 0, 0) \quad R_1 < r < R_2,$$

$$p_1 - p_2 = \frac{\sigma}{R_1},$$

where $W_0$, $R_1$ are constants. This solution represents a perfectly cylindrical jet of constant axial velocity flowing into a quiescent medium. When the jet interface deforms we need to solve the problem in the regions $\mathcal{D}_1 : 0 < r < S(t, z)$ and $\mathcal{D}_2 : S(t, z) < r < R_2$. There are two separate mechanisms of instability present: (i) Kelvin-Helmholtz instability of a cylindrical vortex sheet, (ii) the destabilization of long waves by the circumferential component of the radius of curvature if surface tension acts. We describe the nonlinear evolution by assuming that the axial length scale of interfacial perturbations is large compared to the radial length scale. We note that such long length scales do not arise directly from linear stability analyses of jets (the characteristic length is of the order of the jet radius for capillary dominated flows), but enter the nonlinear evolution through initial interfacial conditions of the form $f(\epsilon z)$ with $\epsilon$ small. The following non-dimensionalizations are appropriate:

$$\overline{r} = \frac{r}{R_1} \quad \overline{z} = \frac{z}{d} \quad \overline{S} = \frac{S}{R_1} \quad \overline{t} = \frac{W_0}{d} t \quad \overline{\phi}_{1,2} = \frac{1}{dW_0} \phi_{1,2} \tag{2.1}$$

Utilization of the scalings (2.1) into the governing equations (omitting the bars) gives:

*Laplace equations in $\mathcal{D}_{1,2}$*

$$\phi_{rr} + \frac{1}{r}\phi_r + \epsilon^2 \phi_{zz} = 0 \tag{2.2}$$

*Kinematic conditions on $r = S$*

$$\phi_{1r} = \epsilon^2 (S_t + \phi_{1z} S_z) \tag{2.3a}$$

$$\phi_{2r} = \epsilon^2 (S_t + \phi_{2z} S_z) \tag{2.3b}$$

*Bernoulli equation on $r = S$*

$$\phi_{1t} + \frac{1}{2}\left(\frac{1}{\epsilon^2}\phi_{1r}^2 + \phi_{1z}^2\right) - \rho\left(\phi_{2t} + \frac{1}{2}\left(\frac{1}{\epsilon^2}\phi_{2r}^2 + \phi_{2z}^2\right)\right) - \frac{1}{2}W_0^2 - W_e$$

$$= -W_e \left[\frac{(1 + \epsilon^2 S_z^2)^{-1/2}}{S} - \frac{\epsilon^2 S_{zz}}{(1 + \epsilon^2 S_z^2)^{1/2}} + \frac{\epsilon^4 S_z^2 S_{zz}}{(1 + \epsilon^2 S_z^2)^{3/2}}\right]. \tag{2.4}$$

*Boundary condition $r = a$*

$$\phi_{2r}(r = a) = 0. \tag{2.5}$$

The constant terms in the Bernoulli equation (2.4) are chosen to satisfy the unperturbed flow. The term on the right hand side is the increment induced by surface tension on the pressure acting across the interface. In (2.2)-(2.5) above, the following nondimensional groups appear

$$\epsilon^2 = \frac{R_1^2}{d^2} \quad \rho = \frac{\rho_2}{\rho_1} \; (\alpha = \frac{1-\rho}{1+\rho}) \quad W_e = \frac{\sigma}{R_1 \rho_1 W_0^2} \quad a = \frac{R_2}{R_1} \; .$$

These parameters are the ratio of radial to axial length scale, the density ratio between outer and inner fluid, the Weber number (ratio between capillary pressure and dynamic pressure), and the ratio between the cylinder radius and the unperturbed jet radius. Equations (2.2)-(2.5) are exact and are a result of a change of variables. For slender jets, however, $\epsilon$ is a small parameter and the following asymptotic expansions are appropriate

$$\phi_{1,2} = \phi_{1,2}^{(0)} + \epsilon^2 \phi_{1,2}^{(1)} + \ldots, \tag{2.6a}$$

$$S = S_0 + \epsilon^2 S_1 + \ldots \quad . \tag{2.6b}$$

Substitution of (2.6a,b) into (2.2) gives the following solutions that satisfy boundedness at the axis ($r = 0$) and the boundary condition at $r = a$

$$\phi_1^{(0)} = B_1(t,z) \quad , \quad \phi_2^{(0)} = B_2(t,z), \tag{2.7}$$

$$\phi_1^{(1)} = -\frac{r^2}{4} B_{1zz} + C_1(t,z) \quad ,$$

$$\phi_2^{(1)} = -\frac{r^2}{4} B_{2zz} + \frac{a^2}{2} B_{2zz} ln(r) + C_2(t,z). \tag{2.8}$$

The functions $B_{1,2}$ and $C_{1,2}$ are to be determined from the kinematic and Bernoulli equations (2.3) and (2.4). The solutions (2.7) for the leading order potentials in $\mathcal{D}_{1,2}$ automatically satisfy (2.3a,b) and (2.4) to leading order. Next, at $O(\epsilon^2)$ and $O(1)$ respectively, equations (2.3a,b) and (2.4) along with the solutions (2.7), (2.8) give

$$-\frac{1}{2} S_0 B_{1zz} = S_{0t} + B_{1z} S_{0z}, \tag{2.9}$$

$$-\frac{1}{2} S_0 B_{2zz} + \frac{a^2}{2S_0} B_{2zz} = S_{0t} + B_{2z} S_{0z}, \tag{2.10}$$

$$B_{1t} + \frac{1}{2} B_{1z}^2 - \rho (B_{2t} + \frac{1}{2} B_{2z}^2) = -\frac{W_e}{S_0} + W_e - \frac{1}{2} W_0^2. \tag{2.11}$$

Equations (2.9)-(2.11) as given above constitute a nonlinear system of three evolutions equations for the three unknowns $S_0, B_1, B_2$. Next we show how they can be reduced to a set of

two coupled equations for the shape of the jet and the axial velocity jump across it. This reduction is useful both mathematically and physically in discussing the pinching process after a finite time (see later).

If we subtract (2.10) from (2.9) to eliminate $S_{0t}$, the result can be readily integrated once with respect to $z$ and enables expression of $B_1$ in terms of $B_2$ by the formula

$$S_0^2 B_{1z} = (S_0^2 - a^2) B_{2z}. \tag{2.12}$$

The unknown function of $t$ that arises from the integration can be taken to be identically equal to zero by choice of appropriate initial conditions (see Papageorgiou and Smith [7] also for a similar theory for two-dimensional wakes). Next we define new variables $W$ and $V$ given by

$$W = B_1 - B_2 \quad , \quad V = B_1 + B_2 \quad , \tag{2.13}$$

which transform (2.12) into

$$\frac{1}{2} a^2 V_z = (\frac{a^2}{2} - S_0^2) W_z \quad . \tag{2.14}$$

The first evolution equation is found by addition of the kinematic conditions (2.9) and (2.10), and elimination of $V$ while the second equation follows from (2.11) again after elimination of $V$ using (2.14). It is convenient to differentiate the resulting Bernoulli equation with respect to $z$ for two reasons: (i) The constant (which can also be a function of time in other configurations) associated with the Bernoulli integral disappears, (ii) the resulting equations involve the functions $S_0^2$ and $W_z$. The latter is seen to be the jump in axial velocity across the deforming vortex sheet and is therefore proportional to the sheet strength. Introducing the variables

$$\eta = \frac{S_0^2}{a^2} \quad , \quad \chi = W_z \quad , \tag{2.15}$$

gives the following coupled system of evolution equations:

$$\eta_t + (\eta\chi - \eta^2\chi)_z = 0, \tag{2.16}$$

$$[\frac{1}{2} + \alpha(\frac{1}{2} - \eta)]\chi_t + \alpha\chi\big(\eta\chi - \eta^2\chi\big)_z$$
$$+\Big([\frac{\alpha}{8} + \frac{\alpha}{2}(\frac{1}{2} - \eta)^2 + \frac{1}{2}(\frac{1}{2} - \eta)]\chi^2\Big)_z = -\frac{W_e}{a(1+\rho)}\left(\frac{1}{\eta^{1/2}}\right)_z . \tag{2.17}$$

Equation (2.17) above, simplifies considerably for the case of equal densities $\alpha = 0$; equation (2.16) is unaffected by density differences and (2.17) for $\alpha = 0$ becomes

$$\chi_t + \Big((\frac{1}{2} - \eta)\chi^2\Big)_z = -\frac{W_e}{a}\left(\frac{1}{\eta^{1/2}}\right)_z . \tag{2.18}$$

Equations (2.16) and (2.17) (or (2.18)) are to be solved subject to prescribed conditions at $t = 0$. To fix matters, we will assume that the flow is periodic in $z$ of period $2\pi$ (a flow of any other period can be scaled to this canonical case by rescaling time).

# 3 Properties of the evolution equations

## 3.1 Conserved quantities

The following are conserved quantities of the evolution

$$I_1 = \int_0^{2\pi} \chi(\frac{1}{2} + \frac{1}{2}\alpha - \alpha\eta)dz \quad , \quad I_2 = \int_0^{2\pi} \eta dz. \tag{3.1a,b}$$

The first conserved quantity is a direct consequence of the Bernoulli equation (2.11). The total energy of the system is also a conserved quantity. The calculations that lead to (3.1c) below are included in Appendix A.

$$I_3 = \int_0^{2\pi} \left(\frac{1}{4}\rho(1-\eta)\eta^2\chi^2 + \frac{1}{4}\eta(1-\eta)^2\chi^2 + \frac{W_e}{a}\eta^{1/2}\right) dz. \tag{3.1c}$$

## 3.2 Equation type

Equations (2.16) and (2.17) can be written in the form

$$\begin{pmatrix} \eta \\ \chi \end{pmatrix}_t + \mathbf{A}(\eta,\chi)\begin{pmatrix} \eta \\ \chi \end{pmatrix}_z = 0,$$

where $\mathbf{A}$ is a $2 \times 2$ matrix with entries which are nonlinear functions of $\eta$ and $\chi$. It is easy to show that the eigenvalues of $\mathbf{A}$, $\lambda$ say, satisfy

$$(\chi - 2\eta\chi - \lambda)\left(\frac{(1+\alpha)\chi - 2\eta\chi}{2\Lambda} - \lambda\right) =$$

$$\frac{\eta(1-\eta)}{\Lambda}\left(\frac{1}{2}(\alpha-1)\chi^2 - \alpha\eta\chi^2 - \frac{W_e}{2a(1+\rho)}\eta^{-3/2}\right),$$

where

$$\Lambda = \frac{1}{2} + \alpha(\frac{1}{2} - \eta).$$

The type of the evolution equations depends on the roots of the polynomial above. In what follows we show that the eigenvalues are complex, in almost all cases, and so the system is elliptic in general. To do this it is enough to show that the discriminant of the quadratic equation is negative. After a series of algebraic manipulations it is shown that the eigenvalues are

$$2\lambda = \chi - 2\eta\chi + \frac{(1+\alpha)\chi - 2\eta\chi}{2\Lambda} \pm (D^2)^{1/2},$$

where

$$D^2 = \frac{4\chi^2\eta(1-\eta)(\alpha^2-1)}{(1+\alpha-2\alpha\eta)^2} - \frac{4W_e\eta(1-\eta)\eta^{-3/2}}{a(1+\rho)(1+\alpha-2\alpha\eta)}.$$

Since $0 < \eta < 1$ and $\alpha^2 \leq 1$ we can conclude that the eigenvalues are complex since $D^2 < 0$. The reason for this is that both terms in the expression for $D^2$ above are negative; this conclusion uses the fact that $2\Lambda = (1 + \alpha - 2\alpha\eta) > 0$ for all relevant values of $\alpha$ and $\eta$.

It is concluded, therefore, that the system is elliptic for almost all values of $\alpha$ and $W_e$. The exceptional case has $\alpha = 1$, $W_e = 0$ which represents a jet in air with zero surface tension yielding real but repeated eigenvalues (further discussion of this case is given in Section 7).

The linear stability spectrum follows from a linearization of the system (3.2) about the unperturbed states. If we write

$$(\chi, \eta) = (1, \frac{1}{a^2}) + \delta(\overline{\chi}, \overline{\eta}) e^{ik(z-ct)},$$

it follows that $c$ is given by $\pm(D^2)^{1/2}$ where $D$ is as given by (3.3) and evaluated at $(\chi, \eta) = (1, \frac{1}{a^2})$. As shown above, $D^2 < 0$ and so instability is obtained with growth rates of $O(k)$, as in Kelvin-Helmholtz instability of a flat vortex sheet for instance. Our aim here is to follow this instability into a fully nonlinear regime with the cylindrical jet interface growing to amplitudes comparable to the unperturbed radius.

# 4 Finite-time singularities: Jet pinching

In this section we consider analytically possible nonlinear terminal states of the evolution equations. It is found that density differences are unimportant in the leading order balances between unsteady and nonlinear terms as a singularity is encountered. It is sufficient to consider equal densities $\rho = 1$ ($\alpha = 0$). The case $\rho \neq 1$ also leads to equations (4.4a,b) below, with $W_e$ replaced by $2W_e$. For equations (2.16) and (2.18), therefore, we postulate that the solutions encounter singularities after a finite time, $t_s$ say, at axial positions $z_s$ and seek to describe the solutions near such points. We make the following ansatz

$$\eta(z,t) = (t_s - t)^\alpha f(\xi) \quad \chi(z,t) = (t_s - t)^\gamma g(\xi)$$
$$\xi = \frac{(z - z_s)}{(t_s - t)^\beta}. \tag{4.1}$$

Physically relevant solutions have $\alpha$ and $\beta$ positive in order to ensure that the interface position does not become unbounded at the critical time, and that the dominant features are due to nonlinear focussing. Under the transformations (4.1) time and space derivatives become

$$\frac{\partial}{\partial t} \rightarrow \frac{\partial}{\partial t} + \frac{\beta\xi}{(t_s - t)} \frac{\partial}{\partial \xi} \quad \frac{\partial}{\partial z} \rightarrow \frac{1}{(t_s - t)^\beta} \frac{\partial}{\partial \xi}. \tag{4.2}$$

Substitution of (4.1), (4.2) in (2.16) and (2.18) along with the usual order-of-magnitude arguments as $t \rightarrow t_s$ from below gives the following expressions relating the constants:

$$\alpha = 4 - 4\beta \quad \gamma = \beta - 1, \tag{4.3}$$

and for $\alpha$ to remain positive we require

$$0 < \beta < 1.$$

Note that this choice of $\beta$ implies a negative $\gamma$ and so the axial velocity jump blows up as the jet radius shrinks to zero.

The conserved integrals (3.1a-c) become to leading order in $(t_s - t)$:

$$I_1 = (t_s - t)^{2\beta-1} \int_{-\infty}^{\infty} g \, d\xi \qquad I_2 = (t_s - t)^{4-3\beta} \int_{-\infty}^{\infty} f \, d\xi$$

$$I_3 = (t_s - t)^{2-\beta} \int_{-\infty}^{\infty} (\frac{1}{4} f g^2 + \frac{W_e}{a} f^{1/2}) \, d\xi. \tag{4.4}$$

Equations (4.4) above represent the local contributions of the focussing region to the three conserved quantities. If the exponents of $(t_s - t)$ are positive the contributions are zero in the limit and no integral constraints need to be placed on possible solutions $f(\xi)$ and $g(\xi)$, whereas if any exponent is negative or zero the corresponding integral it multiplies must vanish. Using (4.3a) we see that the $I_2$ and $I_3$ contributions are zero in the limit. Consideration of the $I_1$ contribution, however, shows that the following constraint is required:

$$\underline{\beta \leq 1/2} \qquad \int_{-\infty}^{\infty} g \, d\xi = 0. \tag{4.5}$$

The governing equations transform to the following one-parameter system of nonlinear ODE's:

$$-4(1-\beta)f + \beta\xi f' + (fg)' = 0, \tag{4.6a}$$

$$(1-\beta)g + \beta\xi g' + \frac{1}{2}(g^2)' = -\frac{W_e}{a}(f^{-1/2})'. \tag{4.6b}$$

In general (4.6a,b) must be solved numerically for different values of $\beta$ and with conditions at $\xi = 0$ (i.e. $z = z_s$) specified for example.

Before the presentation of solutions to (4.6a,b), we note that the same self-similar equations are obtained for the case of a jet in air. Further more, the constraints on $\beta$ imposed by the conserved integrals of the system are preserved and so the solutions that follow apply equally well to jets in air. For completeness the analogous derivation of a jet in air is contained in Appendix B.

# 5 Collapse of cylindrical vortex sheets with zero surface tension.

The equations governing the self-similar break-up structure become:

$$-4(1-\beta)f + \beta\xi f' + (fg)' = 0, \tag{5.1a}$$

$$(1-\beta)g + \beta\xi g' + \frac{1}{2}(g^2)' = 0. \tag{5.1b}$$

The equation for $g$ is nonlinear but is decoupled from that for $f$ which is linear. Once $g$ is determined, the solution for $f$ readily follows:

$$f(\xi) = f_0 \exp\left((1-\beta)\int_0^\xi \frac{5g + 4\beta\xi}{(\beta\xi + g)^2} d\xi\right). \tag{5.2}$$

The main task, therefore, is in the determination of $g$ and classes of exact solutions are constructed next.

An exact solution is readily available for the critical case $\beta = \frac{1}{2}$; (5.1b) can be integrated once to yield a quadratic algebraic equation for $g(\xi)$ which yields the solutions

$$2g_\pm = -\xi \pm \sqrt{\xi^2 + 4g_0^2}, \tag{5.3}$$

where $g_0 = g(0)$. The solution $g_+$ pertains to positive velocity jumps while $g_-$ describes flows with negative jumps. The corresponding solutions for $f$ are

$$f_+ = \frac{f_0}{16 g_0^4} \frac{(\xi + \sqrt{\xi^2 + 4g_0^2})^5}{(\xi^2 + 4g_0^2)^{1/2}}$$

$$f_- = 64 f_0 g_0^6 (\xi + \sqrt{\xi^2 + 4g_0^2})^{-5} (\xi^2 + 4g_0^2)^{-1/2}, \tag{5.4}$$

with $f_0 = f(0)$. The behavior for large $\xi$ is

$$f_+ \sim \frac{f_0}{16 g_0^4}\xi^4 \quad g_+ \sim \frac{g_0^2}{\xi} \quad \xi \to +\infty,$$

$$f_+ \sim 2g_0^6 |\xi|^{-6} \quad g_+ \sim |\xi| \quad \xi \to -\infty.$$

$$f_- \sim 64 g_0^6 f_0 \xi^{-6} \quad g_- \sim -\xi \quad \xi \to +\infty,$$

$$f_- \sim \frac{2f_0}{g_0^4}|\xi|^4 \quad g_- \sim -\frac{g_0^2}{|\xi|} \quad \xi \to -\infty.$$

Even though the solutions $f_\pm(\xi)$ are admissible the corresponding $g_\pm(\xi)$ are not, due to the conservation constraint (4.5) requiring that the integral vanish. This is satisfied by $g(\xi) = g_-(\xi)$ for $\xi < 0$, and $g(\xi) = g_+(\xi)$ for $\xi > 0$, but such solutions are not acceptable since $g(\xi)$ and $f(\xi)$ are now discontinuous at $\xi = 0$, in violation of our slender jet approximation. We reiterate here, that any solutions $f(\xi)$, $g(\xi)$ with bounded derivatives are acceptable singular states of the slender jet equations; unbounded derivatives herald the introduction of shorter scales over which a new acceptable solution may emerge. Such analyses are not pursued further here since we are interested in the construction of pinching solutions.

For any value of $\beta$,

$$g(\xi) = -\xi, \quad f(\xi) = A\xi^{\frac{5-4\beta}{\beta-1}},$$

are exact solutions with $A$ some constant. The solution for $g$ is an odd function of $\xi$ and is consistent with the integral constraint (4.5). For $f(\xi)$ to be acceptable we require boundedness of the first derivative at $\xi = 0$; this is not possible for $\beta < 1$, and this family of solutions is therefore dropped.

For $\beta = 2/3$ another exact solution is found; this is most easily seen by multiplication of (5.1b) by $g$ and integration with respect to $\xi$ which gives

$$(1 - \frac{3}{2}\beta)\int_0^\xi g^2 d\xi + \frac{1}{2}\beta\xi g^2 + \frac{1}{3}g^3 = \frac{1}{3}g_0^3 \quad g_0 = g(0),$$

from which it follows that for $\beta = 2/3$, $g$ satisfies the cubic polynomial

$$g^3 + \xi g^2 - g_0^3 = 0. \tag{5.5}$$

If $g_0 = 0$ the nontrivial solution is $g = -\xi$ with corresponding $f = A\xi^{-7}$ which is singular at the origin and is discarded (see above). Equation (5.5) can have (i) one real root and a pair of complex conjugate roots, (ii) three real roots of which at least two are equal, and (iii) three distinct real roots, depending on the conditions

$$(i)\ Q > 0 \quad (ii)\ Q = 0 \quad (iii)\ Q < 0,$$

$$Q = \frac{1}{4}g_0^3(g_0^3 - \frac{4}{27}\xi^3),$$

respectively. The position $\xi = \xi_c = \frac{3}{4^{1/3}}g_0$ yields $Q = 0$ and is the point above which three distinct solutions exist. At $\xi = \xi_c$ there is a root $g = g_0/4^{1/3}$ and a pair of equal roots $g = -2g_0/4^{1/3}$. A local analysis shows that $g \sim (\xi - 1)^{1/2}$ in the vicinity of the double root indicating that the derivative is infinite at $\xi_c$. The solutions of (5.5) for $g_0^3 = 4/27$ are shown in Figure 1; the dashed line represents $g = -\xi$ which is the asymptotic state of one of the solutions for large $\xi$. Within the context of the long wave theory, the roots with unbounded derivatives are discarded and so a unique acceptable solution exists for $\beta = 2/3$.

The type of solution given above for $\beta = 2/3$ can be generalized to arbitrary values of $\beta$. Under the transformation

$$g(\xi) = \xi G(\xi), \tag{5.6}$$

equation (5.1b) becomes

$$G^\beta(1 + G)^{1-\beta} = \frac{K}{\xi}, \tag{5.7}$$

where $K$ is a constant of integration. Equation (5.7) yields $G$ implicitly in terms of $\xi$. We can rewrite (5.7) in terms of $g$ using (5.6) to give

$$g^\beta(\xi + g)^{1-\beta} = g_0, \tag{5.8}$$

where $g_0 = g(0)$. Equation (5.8) is a generalization of (5.5) to arbitrary values of $\beta$. In particular if $\beta$ is a rational number with $\beta = p/q$ with $p, q$ integers such that $1/2 < \beta < 1$, (5.8) becomes

$$g^p(\xi + g)^{q-p} = g_0^q. \tag{5.9}$$

The values $p = 2$, $q = 3$ yield equation (5.5). We are interested in generating real solutions of (5.9) which are acceptable similarity forms of the breakdown. To do this we begin at $\xi = 0$ where there is one real root and $q - 1$ complex roots if $q$ is odd, or, two equal and opposite real roots and $q - 2$ complex roots if $q$ is even, and follow the appropriate real root as a function of $\xi$ to obtain $g(\xi)$. This can be done for negative $\xi$ also; alternatively the differential equations can be solved directly. This was also done as a check.

The behavior of solutions to (5.1a,b) for large $\xi$ is found to be

$$f \sim \xi^{\frac{4(1-\beta)}{\beta}} \qquad g \sim \xi^{-\frac{1-\beta}{\beta}} \quad \xi \to \infty. \tag{5.10a}$$

The constants of proportionality can be determined numerically. For $\xi \to -\infty$ the equations are analyzed for large positive $\xi_1 = -\xi$ to give the asymptotic forms

$$f \sim (-\xi)^{-1} \qquad g = (-\xi) + \ldots \quad \xi \to -\infty. \tag{5.10b}$$

We note that the constant of proportionality for the decay rate of $f$ is determinable numerically, whereas the constant for the leading order asymptotic behavior for $g$ is equal to unity. These results are confirmed by our numerical solutions described next.

Numerical solutions can be generated for any $\beta$ in the designated range. Here we present a set of solutions for $\beta = 2/3, 4/5, 9/10$. The results are presented in Figures 2, 3 for $f(\xi)$ and $g(\xi)$ respectively. The initial conditions for all solutions are $f(0) = 0.5$, $g(0) = 1.0$. The asymptotic results (5.10a,b) are confirmed by these solutions. The behavior of $g(\xi)$ as $\xi \to -\infty$ predicted above is clearly seen in Figure 8 where the behavior is independent of $\beta$ and the curves collapse to a line of unit slope. Of particular interest are the solutions for $\beta = 4/5$. According to (5.10a), $f(\xi)$ grows linearly for large positive $\xi$ when $\beta = 4/5$. For $\beta < 4/5$ the $f(\xi)$ is concave for large $\xi$ and for $\beta > 4/5$ it is convex. As explained below, viewed from outside the similarity region, the solution for $\beta = 4/5$ represents a conical jet (the radius is a linear function of axial position) while the solutions for $\beta < 4/5$ and $\beta > 4/5$ represent concave and convex jets respectively at the singular time. The convex jet solution which has $\beta = 7/8$ is shown in Figure 4 for $\xi > 0$. The initial conditions are $f(0) = 0.3$, $g(0) = 0.6$. The asymptotic forms (5.10a) are confirmed numerically in Figure 5 by use of a logarithmic plot and a least squares fit of the resulting data to obtain an estimate for the slope. As expected the errors between the exact and the computed value of the slope decrease slowly as the upper limit of integration is increased.

Since the solution for $f$ becomes unbounded for large positive $\xi$ (as does that for $g$ at large negative $\xi$), it is essential to check that these asymptotic values are consistent with the ansatz (4.1); such analysis also provides a qualitative description of the break-up from outside the similarity region. If we substitute the asymptotic forms (5.10a) into (4.1) and express $\xi$ in terms of the physical spatial variable $z - z_s (> 0)$ we find that when viewed from outside the self-similar region, the break-up takes the spatial characteristics

$$\eta \sim (z - z_s)^{\frac{4(1-\beta)}{\beta}} \qquad \chi \sim (z - z_s)^{-\frac{1-\beta}{\beta}}.$$

For $z < z_s$ the asymptotic forms (5.10b) are used to give

$$\eta \sim \frac{(t_s - t)^{4-3\beta}}{(z_s - z)} \qquad \chi \sim \frac{(z_s - z)}{(t_s - t)}.$$

These expressions indicate the geometry of the jet at break-up; the shape is squeezed to a thread as $\xi \to -\infty$ with the radius tending to zero as the singular time is approached (this can be seen from the fact that $1 < 4 - 3\beta < 5/2$) on one side, while it has a concave or convex growth on the right depending on the value of $\beta$. The corresponding velocity jumps tend to infinity and zero respectively at the algebraic rates given above. For example, the exact solution given above for $\beta = 2/3$ gives a parabolic shape at break-up.

# 6 Collapse of cylindrical vortex sheets including surface tension

The governing equations are (4.6a,b). The parameter $W_e/a$ in (4.6b) can be re-scaled to unity by the transformation $f \to (W_e^2/a^2)f$, yielding the normalized form

$$-4(1-\beta)f + \beta\xi f' + (fg)' = 0, \tag{6.1a}$$

$$(1-\beta)g + \beta\xi g' + \frac{1}{2}(g^2)' = -(f^{-1/2})'. \tag{6.1b}$$

Before presentation of numerical solutions it is useful to examine the large $|\xi|$ behavior of the solutions. For large positive $\xi$ we look for solutions of the form

$$f \sim A\xi^m \qquad g \sim B\xi^{-n} \quad m, n > 0. \tag{6.2}$$

Using these expressions in (6.1a) implies

$$m = \frac{4(1-\beta)}{\beta}.$$

The correct value of $n$ which matches the numerical solutions is found by a balance of the linear terms in (6.1b). To illustrate this we write the asymptotic form of (6.1b) according to the scalings (6.2),

$$(1-\beta)B\xi^{-n} - \beta n B\xi^{-n} - B^2 n\xi^{-2n-1} + O(\xi^{-2n-1}) = \frac{m}{2A^{1/2}}\xi^{-\frac{m}{2}-1},$$

with part of the higher order correction terms shown explicitly. If we choose to match the linear terms in $B$ on the left with the surface tension nonlinearity on the right, a value for $n$ is found which makes the constant $B$ negative in contrast to numerical solutions. The correct behavior is determined by matching the linear terms which gives

$$n = \frac{m}{4} = \frac{1-\beta}{\beta}.$$

With this value of $n$ the linear terms (which are the largest terms in the equation) match automatically with $B$ arbitrary. Similar arguments apply for $\xi \to -\infty$ (the analysis is almost identical if we write $\xi_1 = -\xi$ and analyze the equations as $\xi_1 \to \infty$). To summarize, therefore, we find

$$f \sim \xi^{\frac{4(1-\beta)}{\beta}} \qquad g \sim \xi^{-\frac{1-\beta}{\beta}} \qquad \xi \to \infty \tag{6.3a}$$

$$f \sim (-\xi)^{\frac{4(1-\beta)}{\beta}} \qquad g \sim (-\xi)^{-\frac{1-\beta}{\beta}} \qquad \xi \to -\infty \tag{6.3b}$$

Note that the solutions for large positive $\xi$ have the same asymptotic behavior as those corresponding to zero surface tension. As $\xi \to -\infty$, however, the behavior is altered significantly. The consequences of this are discussed after the presentation of numerical solutions.

Equations (6.1a,b) were solved numerically with particular interest in the verification of the asymptotic structures (6.3a,b). The initial conditions used were $f(0) = 1/2$, $g(0) = 1$ with an integration range as large as $(-100, 100)$. Results are presented for the three representative values $\beta = 2/3, 4/5, 9/10$. Figure 6 shows collectively the solutions for $g(\xi)$. The maximum/minimum in $g$ decreases/increases as $\beta$ is increased. A notable feature is that there are two distinct regions, $\xi < \xi_0$, $\xi > \xi_0$ for some value $\xi_0$, where the axial velocity jump is negative and positive respectively. Changing the initial condition so that $g(0) < 0$ for example, indicates that this separation is preserved. Results for the corresponding $f$ solutions are given in Figures 7a,b,c separately due to the large scale differences involved. For $\beta < 4/5$ the computed shape is concave, and the solution for $\beta = 2/3$ has a minimum at $\xi = -0.3$ approximately; the solution corresponding to $\beta = 4/5$ is a critical one with a linear growth at $\pm\infty$ (see Section 5 also), with a minimum radius at $\xi = -0.38$ approximately; solutions having $\beta > 4/5$ are convex in regions sufficiently far away from the origin and the computed solution for $\beta = 9/10$ has a minimum at $\xi = -0.48$ approximately. For the solutions presented here, the position of minimum radius (i.e. the value of $\xi$ which makes

$f(\xi)$ a global minimum) is larger than the positions where the jump in axial velocity (which proportional to $g(\xi)$) is zero.

Next we use the numerical solutions just presented to check the asymptotic forms of the solutions. This is done using logarithmic plots and a least squares fitting of the resulting data. For large positive $\xi$ results are shown in Figures 8a-c for $f$ and $g$ for the three representative values of $\beta$. The agreement is very good and is found to improve as the value of computational "infinity" is increased, as expected. For large negative $\xi$ analogous results with similar accuracy are found and need not be presented here.

As in Section 5, the asymptotic form of the solutions far from the origin enables the qualitative description of the shape at break-down. Considering the shape first, there appear to be three canonical forms at break-down corresponding to the cases (i) $\beta < 4/5$, (ii) $\beta = 4/5$, and (iii) $\beta > 4/5$. For case (i) a concave shape is found at infinity and the jet would tend to pinch forming drops; case (ii) gives linear shapes at infinity and at break-down the jet surface would look like two right circular cones with a common vertex; case (iii) yields jets with shapes which are locally convex in the axial direction. Photographs of experiments in air (see [4], [5]) indicate behavior which fits in with cases (i) and (iii). An additional fact which is evident from the experiments and makes long wave theories like the present one (see also [TK]) useful candidates for break-down prediction, is the validity of the slender jet assumption and in particular the absence of gradient steepening in the shapes at break-down.

# 7 Conclusions

We have developed a nonlinear theory to describe the pinching process of a cylindrical jet of fluid surrounded by a second fluid with possibly different density. The interface between the two fluids can support surface tension. The theory is based on the smallness of the jet radius to a typical axial wavelength of the jet. This excludes jets which try to roll up and such behavior would appear as a slope singularity in our model evolution equations. As an illustration of such behavior, consider the equations (B1), (B2) for a jet in air in the absence of surface tension ($W_e = 0$). Equation (B2) is an inviscid Burgers equation and $\chi$ forms a shock singularity after a finite time (for definiteness we are considering the periodic problem with smooth initial conditions). Similar behavior is found for $\eta$; the slender jet approximation is violated for such solutions since the axial length scale becomes much smaller than the radial one violating the original assumptions used to derive the model. If surface tension is included, however, the equations become elliptic and allow the possibility of admissible pinching solutions described in this article. It is interesting to find that for jets

surrounded by an outer fluid so that the Kelvin-Helmholtz instability mechanism is present, the model equations even in the absence of surface tension are elliptic and pinching solutions can again be constructed.

Finally, we return to the similarity solutions constructed in Sections 5 and 6. There appear to be three canonical breakdown regimes corresponding to (i) $\beta < 4/5$, (ii) $\beta = 4/5$, and $\beta > 4/5$ (see Section 6). In what follows we consider the validity of such solutions within the context of the long wave theory. These equations are derived for the following *unscaled* lengths (stars are used to denote unscaled quantities):

$$z^* \sim \frac{1}{\epsilon} \qquad r^* \sim 1. \tag{7.1}$$

As a finite-time singularity is encountered, it is seen from (4.1) that the length scales over which similarity solutions are constructed are:

$$z^* \sim \frac{(t_s - t)^\beta}{\epsilon} \qquad r^* \sim (t_s - t)^\alpha. \tag{7.2}$$

We know from (4.3) that $\alpha = 4 - 4\beta$ which when substituted into (7.2) along with the ordering $z^* >> r^*$ in order to validate the slender jet approximation, yields the ordering

$$\frac{(t_s - t)^\beta}{\epsilon} >> (t_s - t)^{4-4\beta}. \tag{7.3}$$

The three canonical cases (i)-(iii) described above can be seen in terms of (7.3). It is easily verified that cases (i) and (ii) satisfy (7.3) for all $t$ arbitrarily close to $t_s$. Case (iii), characterized by $\beta > 4/5$, is analyzed by letting $\beta = 4/5 + \delta$ with $\delta > 0$; this requires the ordering

$$(t_s - t)^{5\delta} >> \epsilon \quad or \quad (t_s - t) >> \epsilon^{\frac{1}{5\delta}}. \tag{7.4}$$

Equation (7.4), therefore, defines a range of times for which convex interfacial shapes are formed at break-down. From a physical point of view we expect solutions corresponding to cases (i) and (ii) to be more appropriate when the ordering (7.4) is not observed. Composite or patched solutions are possible, however, whereby for times given by (7.4) a convex drop begins to form which is then matched to a concave or linear shape corresponding to $\beta < 4/5$ and $\beta = 4/5$ respectively, to allow evolution well into the break-down regime without violation of the slender jet ansatz.

# A Derivation of the energy conserved quantity

The flow is governed by the incompressible Euler equations which are conservative and so the total energy of the system is expected to be conserved throughout the evolution. Contributions to the energy come from (i) kinetic energy, (ii) potential energy (in the presence of gravity), (iii) interfacial energy. For a periodic flow of period $d$ (non-periodic flows simply alter the integration limits) the total energy using the dimensional variables of Section 2 is

$$\mathcal{E} = \int_S^{R_2}\int_0^{2\pi}\int_{-d/2}^{d/2}\frac{1}{2}\rho_2|\nabla\phi_2|^2 r dr d\theta dz + \int_0^S\int_0^{2\pi}\int_{-d/2}^{d/2}\frac{1}{2}\rho_1|\nabla\phi_1|^2 r dr d\theta dz$$
$$+\int_S^{R_2}\int_0^{2\pi}\int_{-d/2}^{d/2} g\rho_2 r z dr d\theta dz + \int_0^S\int_0^{2\pi}\int_{d/2}^{d/2} g\rho_1 r z dr d\theta dz$$
$$+\sigma\int_0^{2\pi}\int_{-d/2}^{d/2} S d\theta dz. \qquad (A1)$$

Clearly the potential energy contributions are zero by virtue of the choice of reference frame. Non-dimensionalizing (A1) according to (2.1) (and dropping bars) yields

$$\mathcal{E} = \int_S^a\int_{-1/2}^{1/2}\frac{1}{2}\rho\left(\frac{\phi_r^2}{\epsilon^2}+\phi_z^2\right) r\ dr\ dz + \int_0^S\int_{-1/2}^{1/2}\frac{1}{2}\left(\frac{\phi_r^2}{\epsilon^2}+\phi_z^2\right) r\ dr\ dz$$
$$+W_e\int_{-1/2}^{1/2} S\ dz. \qquad (A2)$$

Making use of expansions (2.6a,b) along with the leading order solutions (2.7) and the change of variables (2.15) yields the following conserved quantity

$$\mathcal{E}_0 = \int_{-1/2}^{1/2}\left(\frac{1}{4}\rho(1-\eta)\eta^2\chi^2 + \frac{1}{4}\eta(1-\eta)^2\chi^2 + \frac{W_e}{a}\eta^{1/2}\right)\ dz, \qquad (A3)$$

where $\mathcal{E}_0$ is a constant. The limits of integration are normalized to be 0 and $2\pi$ as they appear in equation (3.2).

We have shown, but for brevity do not include here, that (A3) is consistent with the evolution equations (2.16), (2.17) for the equal density case. This is achieved by taking the time derivative of (A3) and eliminating $\eta_t$ and $\chi_t$ from (2.16), (2.17) to show that the integrand is an exact $z$-derivative and so the expression is identically zero.

# B Equations for the collapse of a jet in air

The analysis of Section 2 is used with a zero density surrounding fluid which implies that $\phi_2 = 0$. The equations to be solved, to leading order, are (2.9) and (2.11) with $B_2 = 0$. If we define

$$\eta = S_0^2 \qquad \chi = B_{1z},$$

the coupled system becomes

$$\eta_t + (\eta\chi)_z = 0, \tag{B1}$$

$$\chi_t + \frac{1}{2}(\chi^2)_z = -W_e(\eta^{-1/2})_z. \tag{B2}$$

The equations are in conservative form and so the integrals (over space) of $\eta$ and $\chi$ are conserved quantities (c.f. (3.1a,b)). The energy conserved quantity is easily obtained from the results of Appendix A and in particular equation (A2). The result is

$$\mathcal{E}_I = \int_0^{2\pi} \left(\frac{1}{4}\eta\chi^2 + W_e\eta^{1/2}\right) dz. \tag{B3}$$

We note that (B1) and (B2) are equivalent to equations (2.11) and (2.10) of [TK] respectively if (2.10) is differentiated with respect to $z$ and the equations are put in terms of our variables.

As a check, if the time derivative of (B3) is taken and $\eta_t$, $\chi_t$ are eliminated by use of (B1), (B2), the resulting integral is

$$-\frac{1}{4}\int_0^{2\pi} [(\eta\chi^3)_z + W_e(\eta^{1/2}\chi)_z] dz,$$

which is zero, as expected, since it is an exact derivative.

If we look for singular solutions of the form (4.1), the orderings (4.3) emerge as well as the scaled conserved quantities (4.4). Mathematically, therefore, the two problems are equivalent and the same restrictions on $\beta$ apply. The equations governing collapse in the self-similar region are, to leading order, the system (4.6a,b).

# References


[1] Lord Rayleigh, *On the instability of jets*, Proc. London Math. Soc., **10**, (1879) pp. 4-13.

[2] D.B. Bogy, *Drop formation in a circular liquid jet*, Ann. Rev. Fluid Mech., **11**, (1979) pp. 207-228.

[3] S. Chandrasekhar, *Hydrodynamic and Hydromagnetic Stability*, Oxford: Clarendon Press, 1961.

[4] R.J. Donnelly and W. Glaberson, *Experiments on the capillary instability of a liquid jet*, Proc. Roy. Soc., A**290**, (1966) pp. 547-556.

[5] P.G. Drazin and W.H. Reid, *Hydrodynamic Stability*, Cambridge University Press, 1981.

[6] L. Ting and J.B. Keller, *Slender jets and thin sheets with surface tension*, SIAM J. Appl. Math., **50** N0. 6, (1990), pp. 1533-1546.

[7] D.T. Papageorgiou and F.T. Smith, *Nonlinear instability of the wake behind a flat plate placed parallel to a uniform stream*, Proc. Roy. Soc., A**419**, (1988) pp. 1-28.

[8] R. Rotunno, *A note on the stability of a cylindrical vortex sheet*, J. Fluid Mech., **87**, (1978), pp. 761-771.

[9] R.E. Caflisch, *Singularity formation for complex solutions of the 3D incompressible Euler equations*, UCLA CAM Report, (1992).

[10] R.E. Caflisch and X-F. Li, *Lagrangian theory for 3D vortex sheets with axial or helical symmetry*, Transport Theory and Statistical Physics, **21(4-6)**, (1992), pp. 559-578.

[11] R.E. Caflisch, X-F. Li and M.J. Shelley, *The collapse of an axisymmetric swirling vortex sheet*, UCLA CAM Report 92-47, (1992).

[12] R. Grauer and T. Sideris, *Numerical computation of 3d incompressible ideal fluids with swirl*, Phys. Rev. Letters, **25**, (1991), pp. 3511-3514.

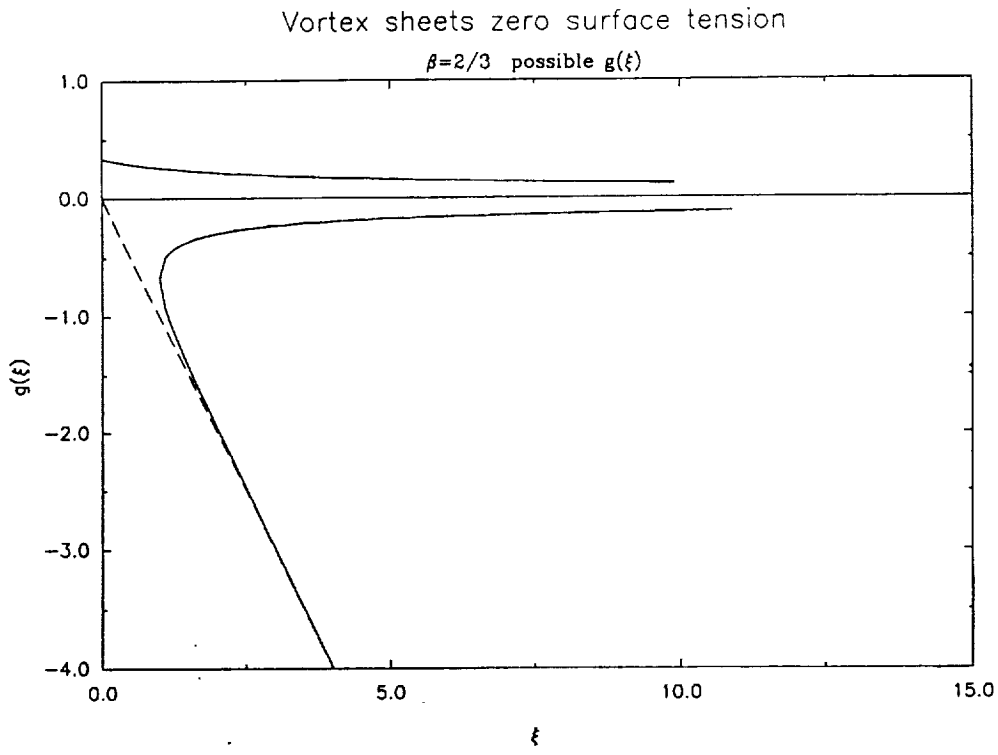


**FIGURE 1** Similarity solutions. Zero surface tension, $W_e = 0$. Possible solutions for scaled axial velocity jump $g(\xi)$ for $\beta = 2/3$.

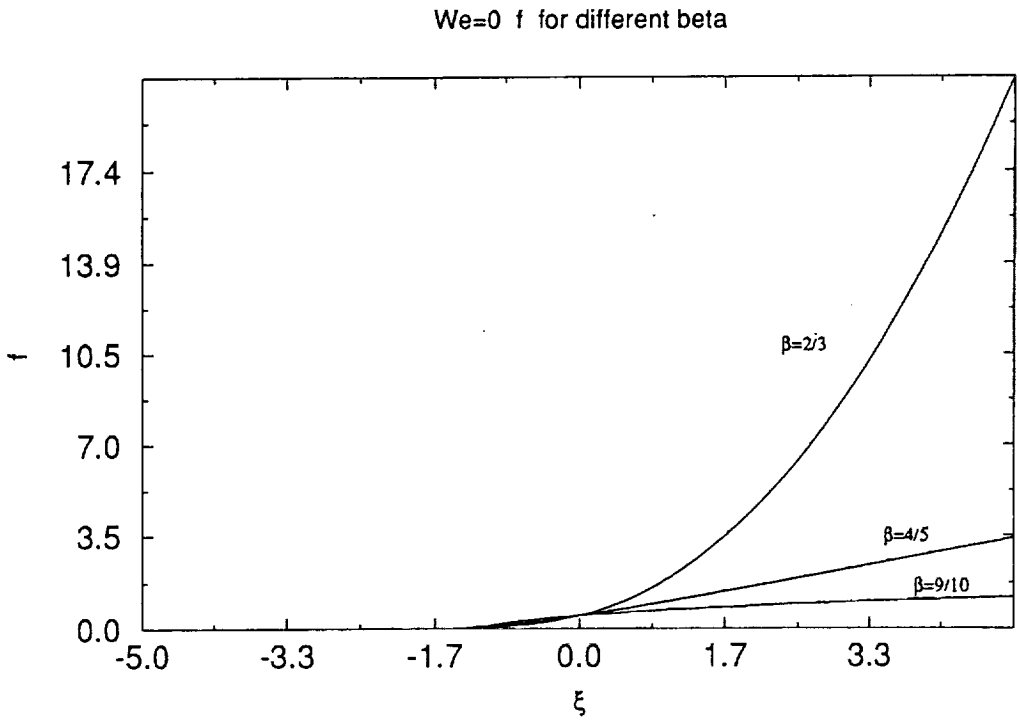


**FIGURE 2** Similarity solutions. Zero surface tension, $W_e = 0$. Scaled interfacial shape $f(\xi)$ for different $\beta = 2/3, 4/5, 9/10$.

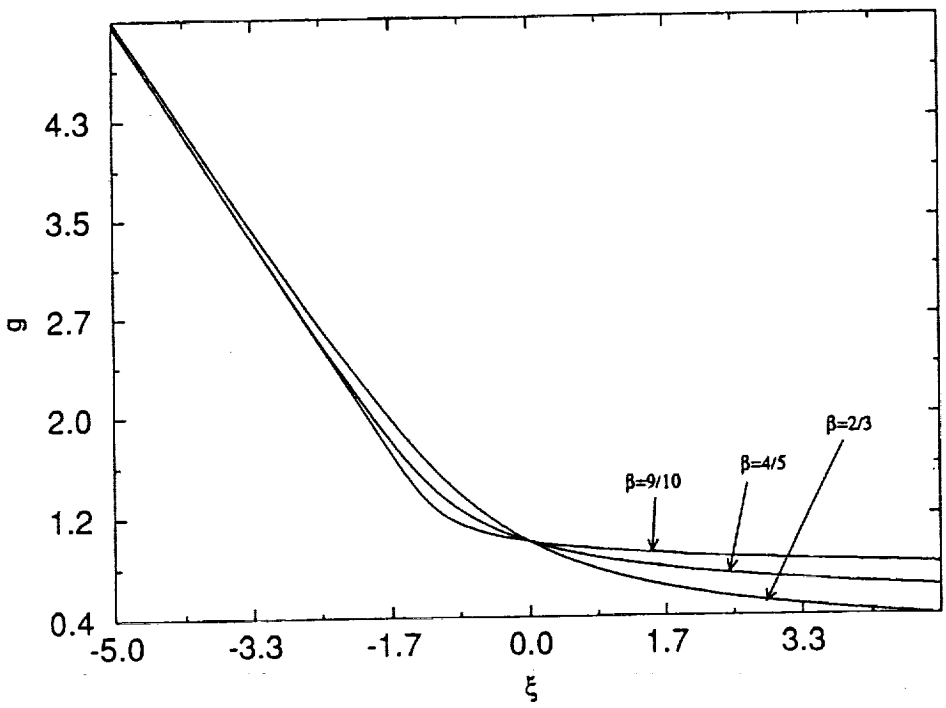


**FIGURE 3** Similarity solutions. Zero surface tension, $W_e = 0$. Scaled axial velocity jump $g(\xi)$ for different $\beta = 2/3, 4/5, 9/10$.

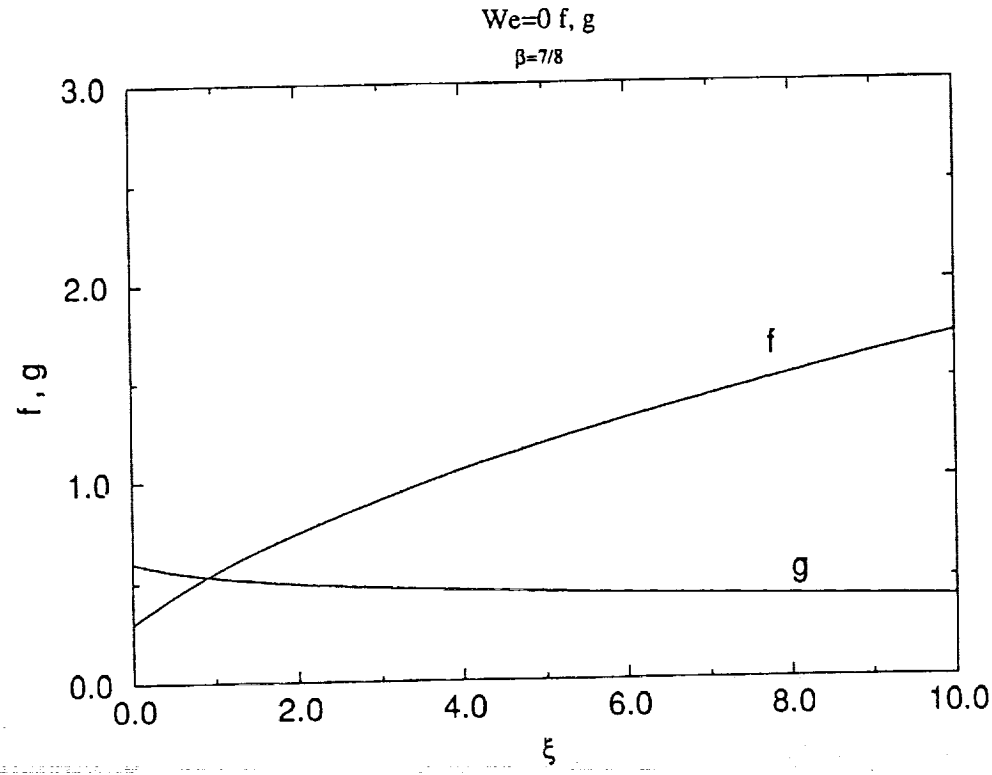


**FIGURE 4** Similarity solutions. Zero surface tension, $W_e = 0$. Detailed view of the solutions $f(\xi)$ and $g(\xi)$ for $\beta = 7/8$, and $\xi > 0$.

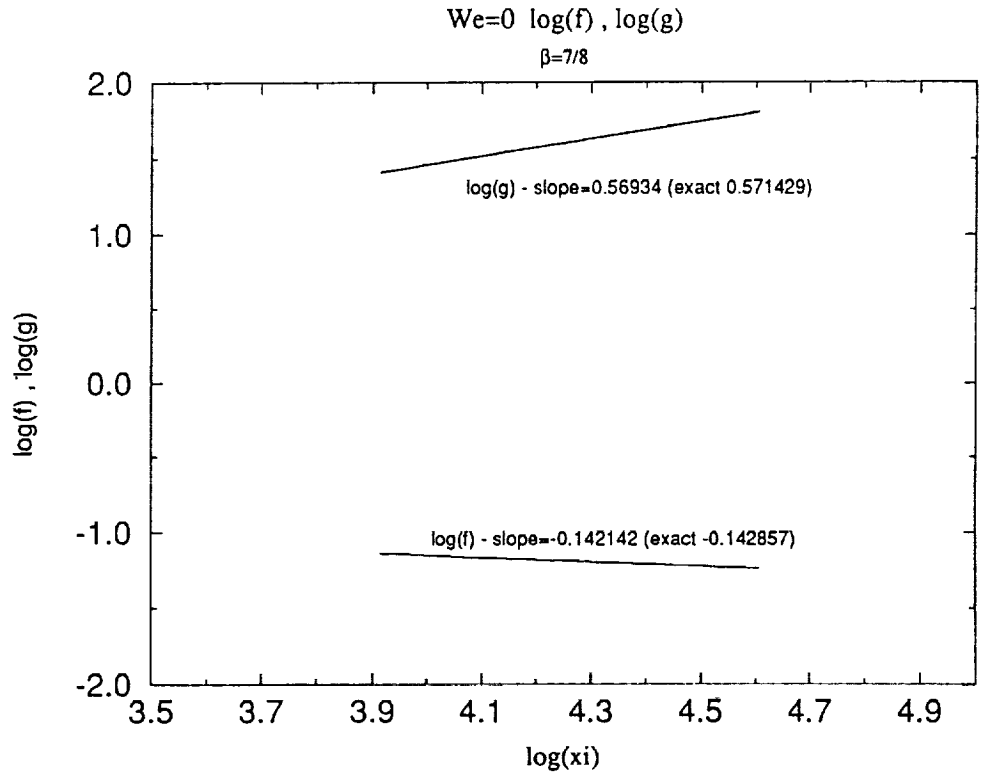


**FIGURE 5** Similarity solutions. Zero surface tension, $W_e = 0$. Logarithmic plots to show the asymptotic behavior of $f(\xi)$ and $g(\xi)$ for large $\xi$ and $\beta = 7/8$. Slopes computed by least squares included on the figure.

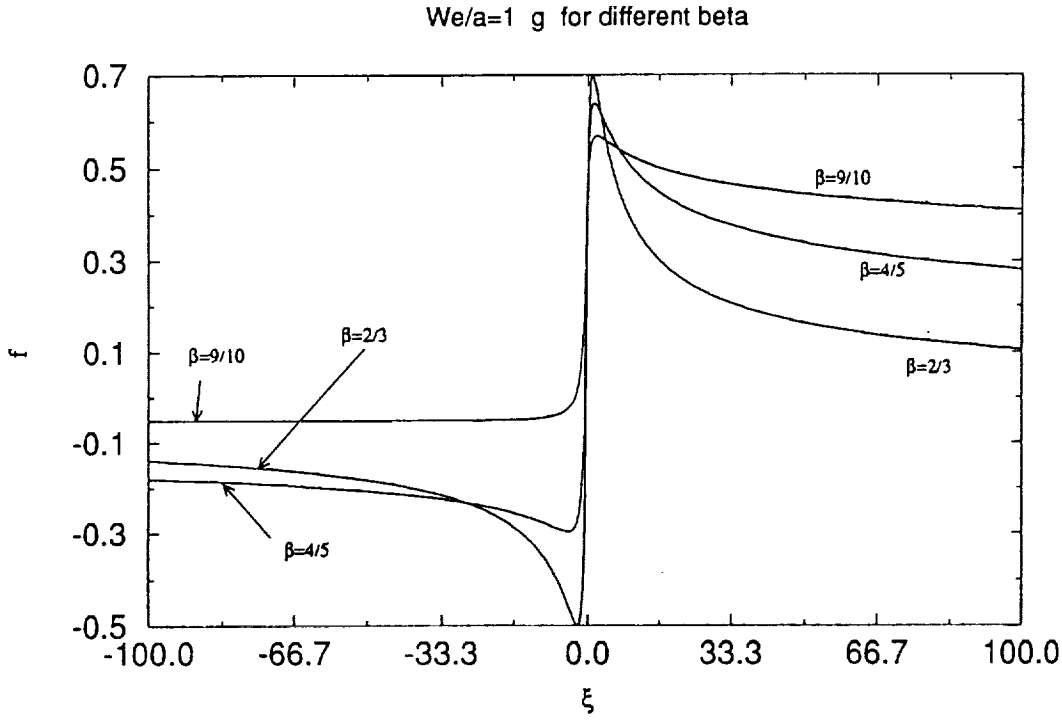


**FIGURE 6** Similarity solutions. Non-zero surface tension, $W_e = 1$. Scaled axial velocity jump $g(\xi)$ for different $\beta = 2/3, 4/5, 9/10$.

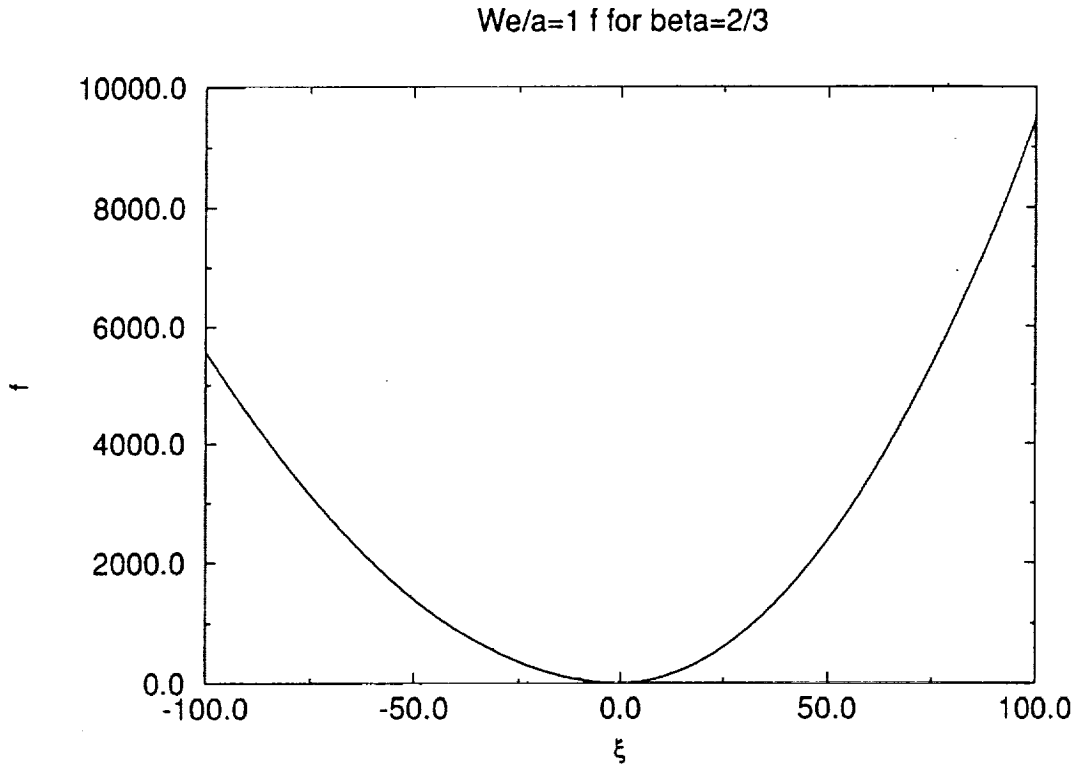


(a)

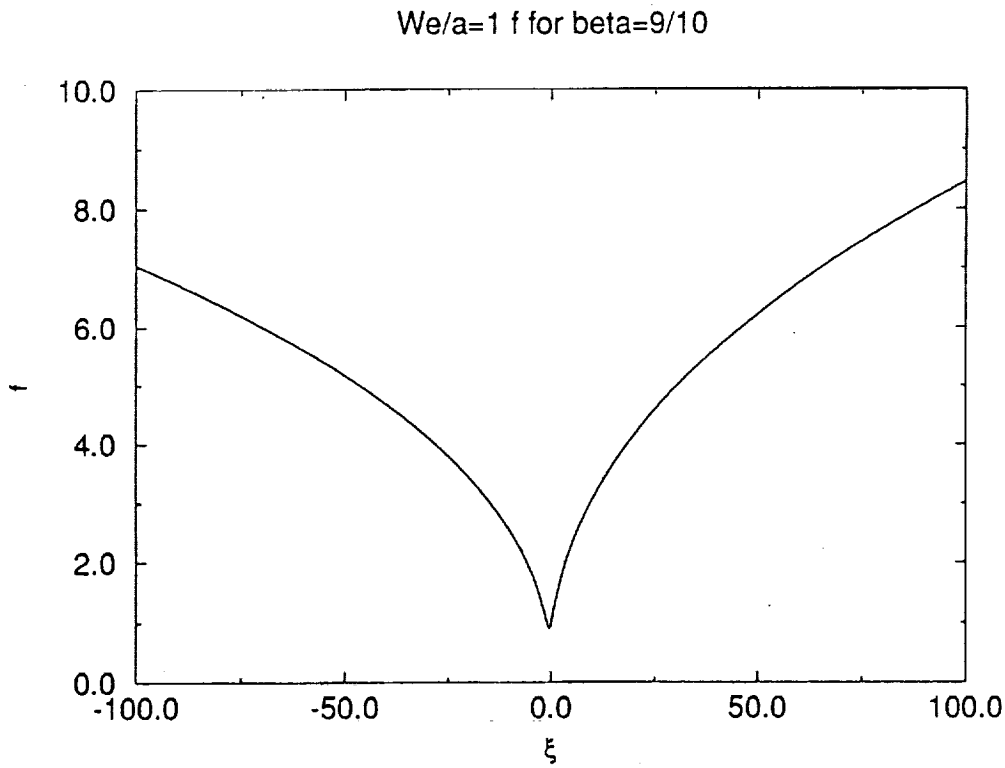


(b)

**FIGURE 7** Similarity solutions. Non-zero surface tension, $W_e = 1$. Scaled interfacial shape $f(\xi)$ for different $\beta$; (a) $\beta = 2/3$, (b) $\beta = 4/5$, (c) $\beta = 9/10$.

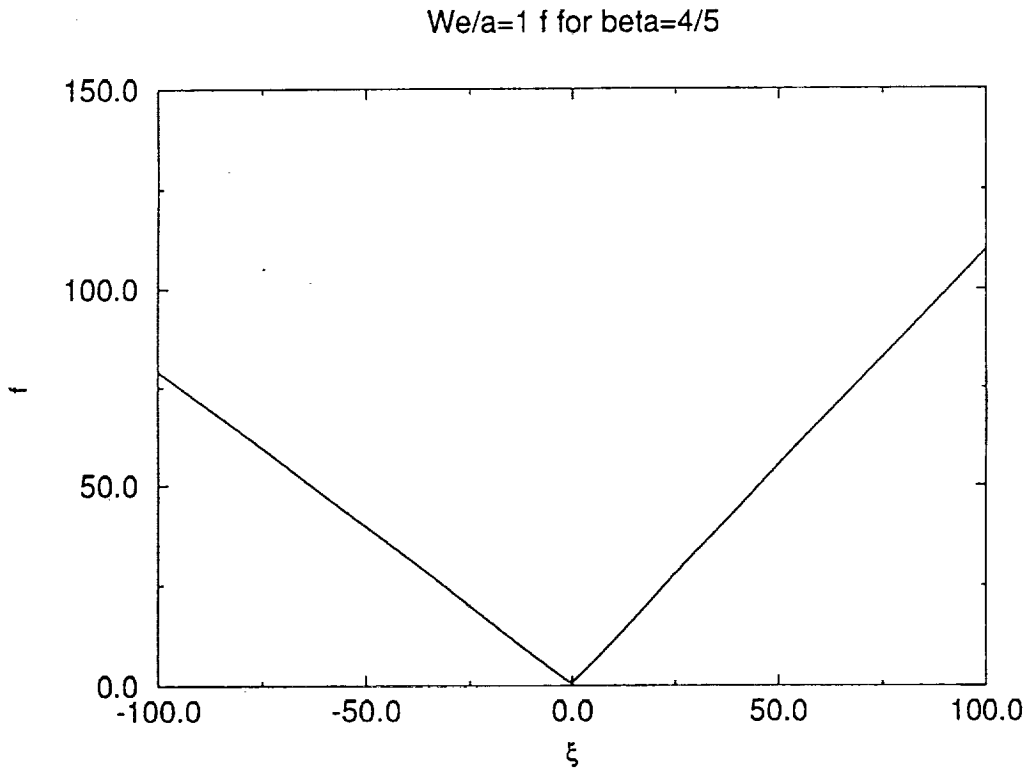


**Figure 7c**

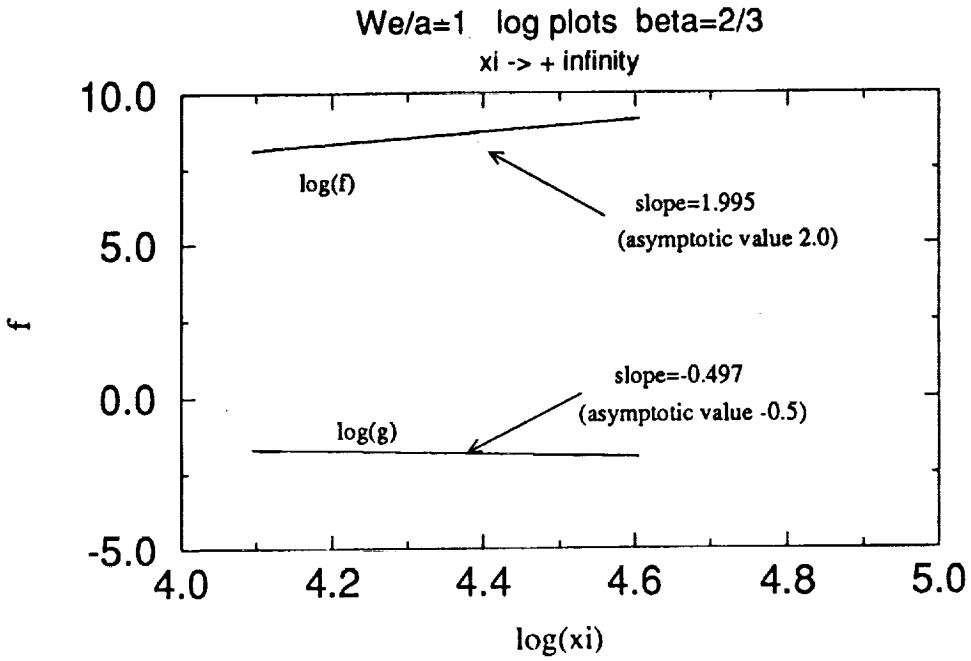


(a)

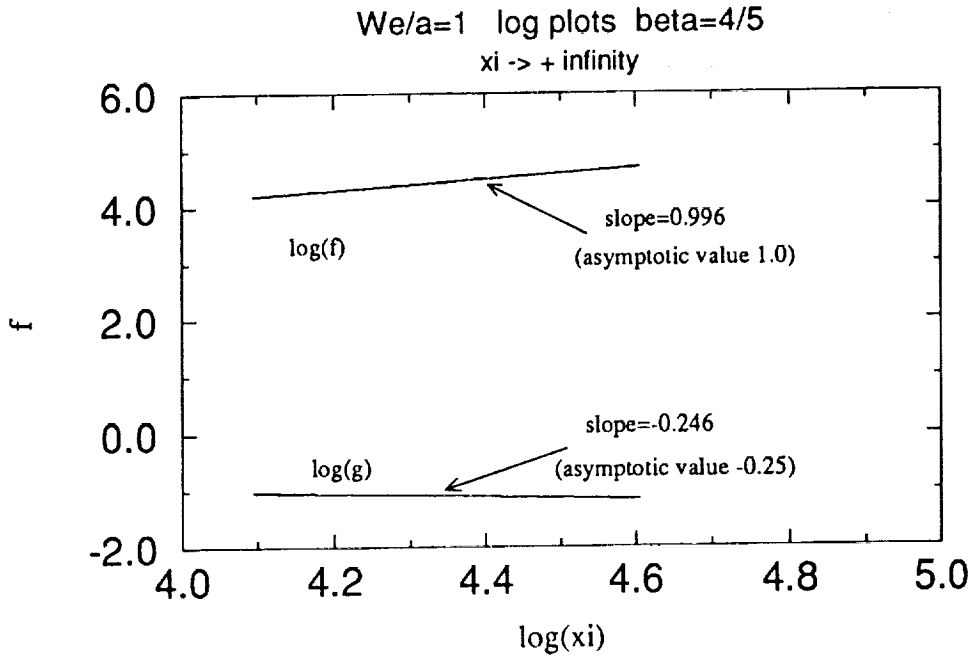


(b)

**FIGURE 8** Similarity solutions. Non-zero surface tension, $W_e = 1$. Logarithmic plots to confirm asymptotic states for large $\xi$. Behavior of $f(\xi)$ and $g(\xi)$ for different $\beta$; (a) $\beta = 2/3$, (b) $\beta = 4/5$, (c) $\beta = 9/10$. Slopes computed by least squares included on the figure.

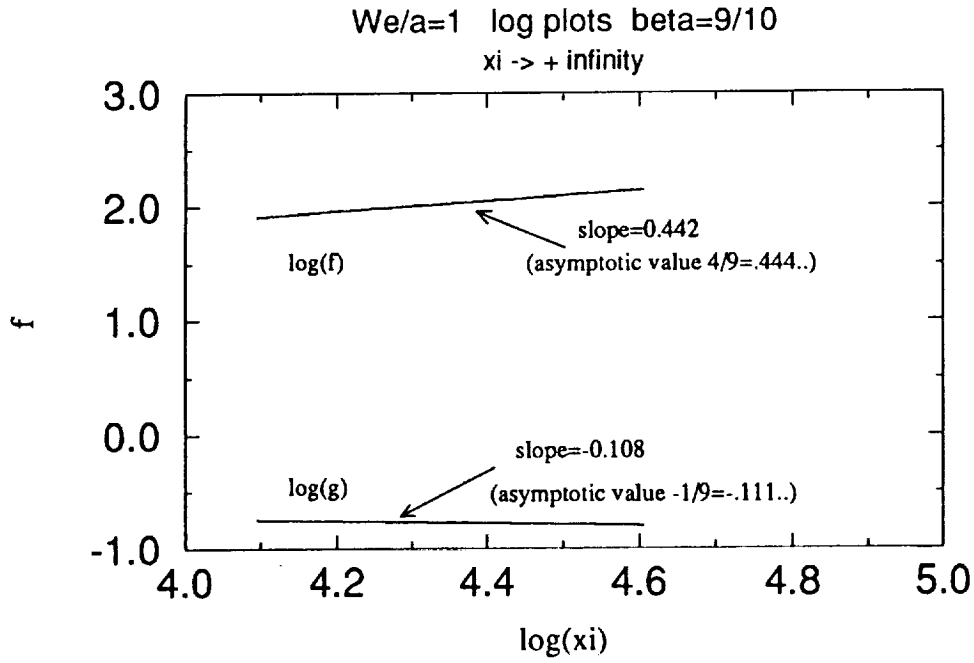
We/a=1 log plots beta=9/10
xi -> + infinity
3.0
2.0
1.0
0.0
-1.0
f
4.0
4.2
4.4
4.6
4.8
5.0
log(xi)
log(f)
slope=0.442
(asymptotic value 4/9=.444..)
log(g)
slope=-0.108
(asymptotic value -1/9=-.111..)

**Figure 8c**

# REPORT DOCUMENTATION PAGE

*Form Approved*
*OMB No. 0704-0188*



| 1. AGENCY USE ONLY *(Leave blank)* | 2. REPORT DATE | 3. REPORT TYPE AND DATES COVERED |
|---|---|---|
| | June 1993 | Contractor Report |

**4. TITLE AND SUBTITLE**
PINCHING SOLUTIONS OF SLENDER CYLINDRICAL JETS

**5. FUNDING NUMBERS**
C NAS1-19480
C NAS1-18605
WU 505-90-52-01

**6. AUTHOR(S)**
Demetrios T. Papageorgiou
Oscar Orellana

**7. PERFORMING ORGANIZATION NAME(S) AND ADDRESS(ES)**
Institute for Computer Applications in Science and Engineering
Mail Stop 132C, NASA Langley Research Center
Hampton, VA 23681-0001

**8. PERFORMING ORGANIZATION REPORT NUMBER**
ICASE Report No. 93-32

**9. SPONSORING/MONITORING AGENCY NAME(S) AND ADDRESS(ES)**
National Aeronautics and Space Administration
Langley Research Center
Hampton, VA 23681-0001

**10. SPONSORING/MONITORING AGENCY REPORT NUMBER**
NASA CR-191482
ICASE Report No. 93-32

**11. SUPPLEMENTARY NOTES**
Langley Technical Monitor: Michael F. Card
Final Report

Submitted to SIAM Journal on Applied Mathematics

**12a. DISTRIBUTION/AVAILABILITY STATEMENT**
Unclassified - Unlimited

Subject Category 34

**12b. DISTRIBUTION CODE**

**13. ABSTRACT** *(Maximum 200 words)*

Simplified equations for slender jets are derived for a circular jet of one fluid flowing into an ambient second fluid, the flow being confined in a circular tank. Inviscid flows are studied which include both surface tension effects and Kelvin-Helmholtz instability. For slender jets a coupled nonlinear system of equations is found for the jet shape and the axial velocity jump across it. The equations can break down after a finite fime and similarity solutions are constructed, and studied analytically and numerically. The break-ups found pertain to the jet pinching after a finite time, without violation of the slender jet ansatz. The system is conservative and admissible singular solutions are those which conserve the total energy, mass and momentum. Such solutions are constructed analytically and numerically, and in the case of vortex sheets with no surface tension certain solutions are given in closed form.

**14. SUBJECT TERMS**
circular jets; singularities; pinching solutions

**15. NUMBER OF PAGES**
29

**16. PRICE CODE**
A03

| 17. SECURITY CLASSIFICATION OF REPORT | 18. SECURITY CLASSIFICATION OF THIS PAGE | 19. SECURITY CLASSIFICATION OF ABSTRACT | 20. LIMITATION OF ABSTRACT |
|---|---|---|---|
| Unclassified | Unclassified | | |

NSN 7540-01-280-5500

Standard Form 298 (Rev. 2-89)
Prescribed by ANSI Std Z39-18
298-102

☆U.S. GOVERNMENT PRINTING OFFICE: 1993 - 728-064/86030